Urban adaptation can roll back warming of emerging megapolitan regions

Matei Georgescu[a,1], Philip E. Morefield[b], Britta G. Bierwagen[b], and Christopher P. Weaver[b]

[a]School of Geographical Sciences and Urban Planning, Global Institute of Sustainability, Arizona State University, Tempe, AZ 85287; and [b]National Center for Environmental Assessment, Office of Research and Development, US Environmental Protection Agency, Washington, DC 20460

Edited by Susan Hanson, Clark University, Worcester, MA, and approved January 15, 2014 (received for review November 27, 2013)

Modeling results incorporating several distinct urban expansion futures for the United States in 2100 show that, in the absence of any adaptive urban design, megapolitan expansion, alone and separate from greenhouse gas-induced forcing, can be expected to raise near-surface temperatures 1–2 °C not just at the scale of individual cities but over large regional swaths of the country. This warming is a significant fraction of the 21st century greenhouse gas-induced climate change simulated by global climate models. Using a suite of regional climate simulations, we assessed the efficacy of commonly proposed urban adaptation strategies, such as green, cool roof, and hybrid approaches, to ameliorate the warming. Our results quantify how judicious choices in urban planning and design cannot only counteract the climatological impacts of the urban expansion itself but also, can, in fact, even offset a significant percentage of future greenhouse warming over large scales. Our results also reveal tradeoffs among different adaptation options for some regions, showing the need for geographically appropriate strategies rather than one size fits all solutions.

sustainability | mitigation | land-use change | urbanization | urban climate

Urban areas are hot spots that drive multisector environmental change (1, 2). Consumption and production of resources for use within urban environments have local and remote implications for ecosystem services, hydroclimate, energy provision, health, and other factors of human wellbeing (1, 3). In semiarid regions, continued conversion of existing lands to urban landscapes has the potential to drive significant local and regional climate change, compounding global warming (4). At the same time, how cities choose to expand and develop will be critical to defining how successful society will be in adapting to global change. Because cities are, in a real sense, fundamental units of both climate change adaptation and mitigation, development choices in the coming century will lead to either significant exacerbation or significant reduction in the impacts of global change (5). In this study, we explore the sensitivity of regional climate to megapolitan expansion at a nationwide scale across the United States for a range of built environment growth and adaptation scenarios. This work advances the broader dialogue about global climate change, urban resilience, the interface between adaptation and mitigation, tradeoffs among strategies, and sustainability.

The United States is the world's third most populous nation, currently adding one person every 13 s to an estimated December of 2012 population of 315 million (6). [The net gain of one person every 13 s accounts for one birth per 8 s (gain), one death per 12 s (loss), and one international migrant per 44 s (gain) (6).] US population projections for 2100 range from 380 [a value likely to be surpassed by midcentury; current 2050 estimates indicate a US population of 422.5 million (7)] to 690 million inhabitants, leading to 208,000–261,000 km^2 of new urban land use relative to 2000 (5). Assessment of regional environmental impacts caused by urban expansion is essential before large-scale landscape modification to help guide and inform more sustainable pathways (4). Among these potential impacts are significant changes in climate. It is well-understood that land use change can have important impacts on local weather and climate (8–10), although the potential for impacts at large regional, continental, and even global scales has been less well-studied (11).

For example, one direct impact of converting natural or cultivated lands to cities is the urban heat island effect (12), which swells from local to regional heat islands as distinct metropolitan complexes grow and merge into megapolitan areas (13). These impacts, however, are not uniform in space and time, with significant seasonal and geographic variability. Any comprehensive examination of urban-induced climate change must, therefore, examine a range of urban forms and footprints across a spectrum of geographies and climates to assess regionally specific impacts of megapolitan emergence and prioritize regionally appropriate adaptation strategies.

Here, we combine high-resolution atmospheric modeling with spatially explicit scenarios of urban expansion for the contiguous United States in 2100 to examine potential regional-scale hydroclimatic impacts associated with emerging megapolitan areas. This national-scale modeling structure allows us to capture synergistic effects associated with polycentric regions of large-scale urban growth, highlighting key emerging urban areas rather than predefining such areas and potentially missing strategic adaptation opportunities in certain regions. Comparison of several plausible urban growth futures with climate change effects offers an unprecedented exploration of ranges of impacts and adaptation strategies.

The advanced research version of the weather research and forecasting model coupled to an urban canopy model (WRF) (14) incorporates the range of urban expansion scenarios and adaptation strategies used in this study. The use of WRF is well-established, spanning from urban (15) to renewable energy (16)

Significance

Conversion to urban landforms has consequences for regional climate and the many inhabitants living within the built environment. The purpose of our investigation was to explore hydroclimatic impacts of 21st century urban expansion across the United States and examine the efficacy of commonly proposed urban adaptation strategies in context of long-term global climate change. We show that, in the absence of any adaptive urban design, urban expansion across the United States imparts warming over large regional swaths of the country that is a significant fraction of anticipated temperature increases resulting from greenhouse gas-induced warming. Adapting to urban-induced climate change is geographically dependent, and the robust analysis that we present offers insights into optimal approaches and anticipated tradeoffs associated with varying expansion pathways.

Author contributions: M.G. designed research; M.G. performed research; M.G., P.E.M., B.G.B., and C.P.W. analyzed data; and M.G., P.E.M., B.G.B., and C.P.W. wrote the paper.

The authors declare no conflict of interest.

This article is a PNAS Direct Submission.

Freely available online through the PNAS open access option.

[1]To whom correspondence should be addressed. E-mail: Matei.Georgescu@asu.edu.

This article contains supporting information online at www.pnas.org/lookup/suppl/doi:10.1073/pnas.1322280111/-/DCSupplemental.

applications, and focused on short (i.e., subseasonal) to longer-term (i.e., multiyear) integrations. We incorporate a range of urban expansion scenarios and adaptation strategies (*SI Appendix*) for the conterminous United States to represent urbanization-induced landscape change into our modeling framework (5). We carried out multiyear (8 y) and multimember (three members) simulations at 20-km horizontal grid spacing for the conterminous United States using maximum (A2; this scenario corresponds to 690 million inhabitants) and minimum (B1; this scenario corresponds to 380 million inhabitants) expansion scenarios and compared them with experiments using a modern day urban representation (control).

The Integrated Climate and Land Use Scenarios (ICLUS) project of the US Environmental Protection Agency (17) created the scenarios of urban expansion. The ICLUS project produced spatially resolved scenarios of land use change for the conterminous United States that are consistent with the projections of global change described in the Special Report on Emissions Scenarios by the Intergovernmental Panel on Climate Change (18). The Special Report on Emissions Scenarios economic, social, and demographic qualitative storylines inform the parameters of the ICLUS demographic and spatial allocation models (5, 17). Bounded by US census population projections, ICLUS uses cohort component and spatial interaction models to distribute both domestic and international migrants among US counties. A decoupled spatial allocation model uses empirical measures of household size, housing density, and accessibility to then allocate new housing units across the landscape at 1-ha spatial resolution.

The ICLUS model projects continuous values of housing density that span common perceptions of rural to urban densities. Characterizing urbanness in this manner (i.e., structural) is fundamentally different compared to derivations from the National Land Cover Database (NLCD) (19) or the Moderate Resolution Imaging Spectroradiometer (MODIS) (i.e., spectral), normally used as input for urban modeling applications in the United States. For this study, we spatially aggregated ICLUS housing density projections from continuous values into four classes: commercial/industrial, urban + suburban, exurban, and undeveloped. The commercial/industrial pixels are highly developed urban areas that we estimate to be >50% nonresidential land uses. ICLUS does not model increases or decreases in this category over time. The urban + suburban pixels corresponded to a density of <2 acres per housing unit; exurban corresponded to a density between 2 and 40 acres per housing unit, and undeveloped included a density of >40 acres per housing unit. These housing density thresholds are frequently, although not exclusively, designated as critical in peer-reviewed literature and consistent with other analyses incorporating the ICLUS housing density projections (5). Relative to a year 2000 baseline, the A2 and B1 ICLUS projections correspond to the most and least amounts of urban expansion, respectively, in the year 2100, and land use grids were created using the above classification to model those respective changes (Table 1). All simulations were conducted using 2001–2008 climate (*SI Appendix*).

Table 1. Naming convention of experiments

Control	Baseline urban extent
A2 ICLUS	Maximum urban expansion
B1 ICLUS	Minimum urban expansion
A2 green roofs	As A2 ICLUS with green roofs
A2 cool roofs	As A2 ICLUS with cool roofs
A2 green–albedo	As A2 ICLUS with hybrid roofs

All experiments were repeated three times (i.e., three ensemble members), with variable spin-up time using 2001–2008 climate. *SI Appendix*, Tables S1 and S2 shows additional details on experiments. A2 cool roofs, the same as A2 ICLUS experiments but with the incorporation of cool roofs for all urban areas; A2 green–albedo, the same as A2 ICLUS experiments but with the incorporation of reflective green roofs for all urban areas; A2 green roofs, the same as A2 ICLUS experiments but with the incorporation of green roofs for all urban areas; A2 ICLUS, experiments using projected A2 ICLUS urban representation for year 2100; B1 ICLUS, experiments using projected B1 ICLUS urban representation for year 2100; control, control experiments using ICLUS urban representation for year 2000.

Summertime urban-induced warming for the A2 expansion scenario is in the range of 1–2 °C for all urban regions, although some areas (e.g., portions of the Chicago/Detroit area) undergo maximum warming in excess of 3 °C locally (Fig. 1). Humid areas (e.g., Florida) show warming of reduced magnitude compared

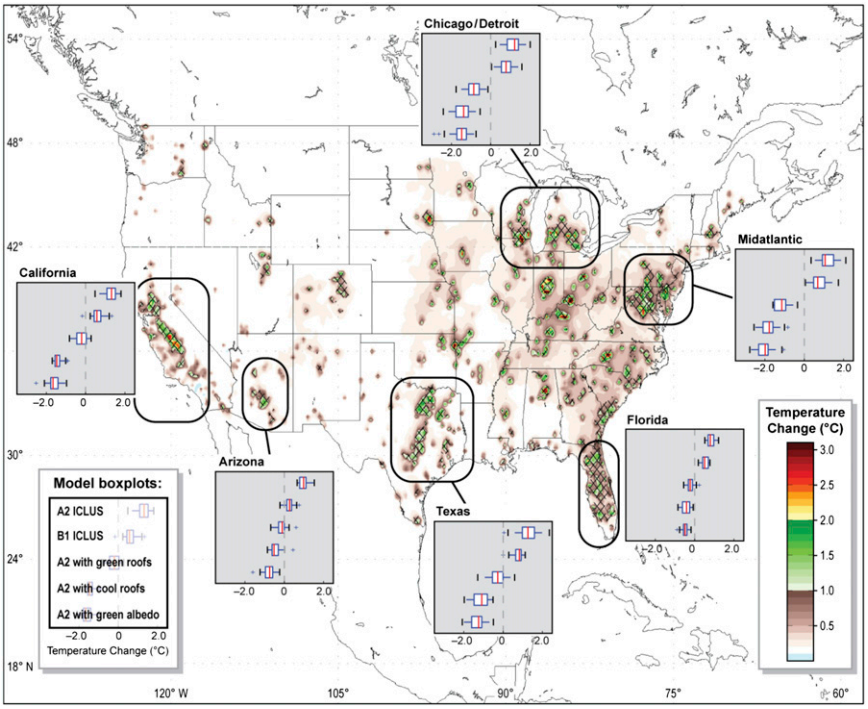

Fig. 1. Simulated June–July–August (JJA) 2-m air temperature difference between A2 and control (°C). Black hatching indicates differences that are virtually certain (greater than 99% probability) to be significant according to the pairwise comparison test (*SI Appendix*). Estimated impacts of all expansion and adaptation scenarios for indicated urban areas are shown as *Insets*, with black ovals outlining each region. Red lines show median impacts; blue box bars show first and third quartiles, and whiskers represent 1.5 times the interquartile range from 24 simulated summers. For each region, box plots indicate differences between A2 and control, B1 and control, A2 green roofs and control, A2 cool roofs and control, and A2 with green–albedo roofs and control from top to bottom, respectively.

with regions experiencing a prolonged dry season, such as the low-lying Mediterranean climates of the Central California Valley. The constrained urban growth pathway (i.e., B1 scenario) has reduced urban-induced warming by about one-third to one-half compared with that for the A2 scenario (Fig.1 and *SI Appendix*, Fig. S4).

The suite of adaptation strategies considered allows examination of the potential to reduce urban-induced warming. Therefore, we repeated all A2 urban expansion experiments using 100% deployment of (*i*) cool roofs (i.e., highly reflective), (*ii*) green roofs (i.e., highly transpiring), and (*iii*) a hypothetical approach incorporating the reflective and transpiring properties of cool and green roofs (green–albedo) (Table 1) over all urban areas. For all megapolitan areas, the trio of adaptation approaches entirely offsets urban-induced warming (Fig. 1). Simulated cooling for each urban region, however, is greater for the cool roofs relative to the green roofs, although this difference is accentuated over drier relative to humid regimes (e.g., adoption of cool roofs leads to about 0.2 °C additional cooling relative to green roofs over Florida but an additional 1.2 °C for California). The deployment of green–albedo roofs leads to a relatively small additional cooling over cool roofs (generally less than 0.3 °C), illustrating an apparent saturation of built environment adaptation at the urban scale. Urban-induced springtime warming is of similar magnitude relative to the summer season, and a persistent pattern of adaptation impacts is evident, with enhanced capability for urban air temperature reduction with cool relative to green roofs (*SI Appendix*, Fig. S5). Expansion scenarios and adaptation strategies exhibit seasonal dependency, because urban-induced warming is reduced for fall and winter (*SI Appendix*, Figs. S6–S8), consistent with recent modeling (20) and remote sensing (21) work for the United States. The adoption of cool roofs promotes enhanced cooling during winter, an effect that could prompt increased energy demand to warm indoor environments (e.g., cooling of about 1.5 °C relative to control for the Mid-Atlantic region) (*SI Appendix*, Table S3). Wintertime cooling is apparent for all regions using cool and green–albedo strategies, but it is not evident for adoption of green

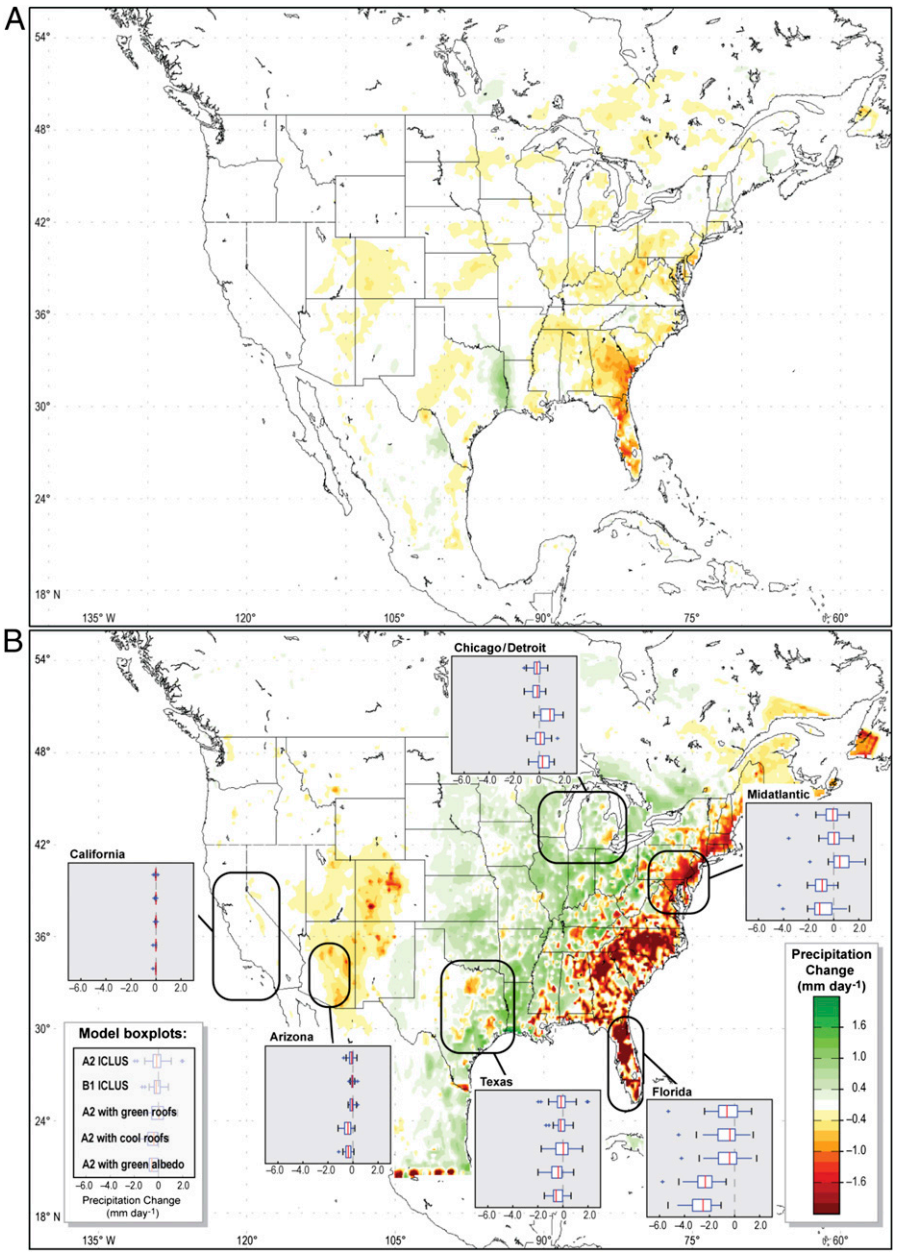

Fig. 2. Simulated JJA precipitation difference between (*A*) A2 and control and (*B*) cool roofs and control. Units are millimeters day^{-1}. Calculations for *Insets* in *B* are performed only for statistically significant grid cells as described and illustrated in Fig. 1.

roofs, because the addition of water vapor promotes warming (generally not exceeding 0.5 °C relative to control) in newly expanded urban regions.

The simulated decrease in evapotranspiration over regions converted to urban landscapes (*SI Appendix*, Figs. S9–S12) is in agreement with prior results showing warmer and drier regional environmental conditions on built environment expansion (4). The A2 expansion pathway indicates reductions in summertime precipitation of about 1 mm d^{-1} that are largely confined to portions of the southeastern United States and Florida, with minimal impacts elsewhere (Fig. 2*A*). Cool roof implementation shows a pronounced decrease in precipitation between 2 and 4 mm d^{-1} along a corridor extending from Florida to the northeastern United States and reduced, although still important, impacts evident for the monsoon states of the southwestern United States (Fig. 2*B*). The simulated decrease in precipitation (for example, over Florida, 24 of 24 simulated summers experience a decrease in total precipitation when deploying cool roofs for the A2 expansion scenario relative to control) is expected to have implications for water demand and scarcity for humans, power generation from stream flow, and aquatic ecosystems (e.g., fisheries, recreation, etc.). These results are in agreement with recent regional- (20) and global-scale modeling studies (22) indicating unintended hydroclimatic consequences associated with large-scale cool roofs deployment, and they are in contrast to impacts associated with green roof implementation, showing a tendency for increasing precipitation for Mid-Atlantic and Chicago/Detroit regions (Fig. 2*B*). Increased central US plains precipitation, apparent during the majority of simulated summers, is potentially linked to pathways of western US moisture redistribution and modulation of regional water cycle dynamics associated with land–atmosphere coupling (23, 24), supporting previous research indicating the possibility of nonlocal hydroclimatic impacts owing to large-scale urbanization (4). Cool roof deployment impacts on precipitation are greatest during summer when land–atmosphere coupling strength is greatest (24), with reduced effects during other seasons (*SI Appendix*, Figs. S13–S15). Policy options focused on adaptation to urban-induced warming should recognize the importance of solutions that also address hydroclimatic implications and encourage comprehensive tradeoff assessments (25), which consider multiscale environmental and multisector socioeconomic elements as well as nonlocal implications, rather than proposed one size fits all policies.

The contribution of urban relative to global warming during summer is locally important, irrespective of megapolitan expansion or emissions pathway (Fig. 3). However, the relative importance of urban warming is consistently greatest for the B1 [corresponding to the Representative Concentration Pathway 2.6 (RCP2.6)] scenario because of considerably reduced greenhouse gas emissions for this storyline and hence, a relatively stronger signal of urban warming. This result emphasizes the need to implement built environment adaptation strategies that control urban temperature impacts, regardless of whether carbon emissions are kept in check. For maximum expansion and greenhouse gas emission scenarios, the regional contribution of urban warming ranges between 15% (Chicago/Detroit region) and 27% (California), with peak local contributions being ∼50% of the simulated future greenhouse gas-induced warming signal. Although the relative contribution of urban-induced warming is somewhat lower for the remaining seasons (*SI Appendix*, Figs. S16–S18), the built environment remains an important element of all megapolitan areas' regional climate, highlighting the need for comprehensive climate change policies that incorporate land-based solutions and extend beyond the nearly exclusive focus of carbon-based approaches (26).

Despite the inherent uncertainties associated with any modeling approach, our national-level analysis reveals the importance of tradeoff assessment (e.g., changes in seasonal energy

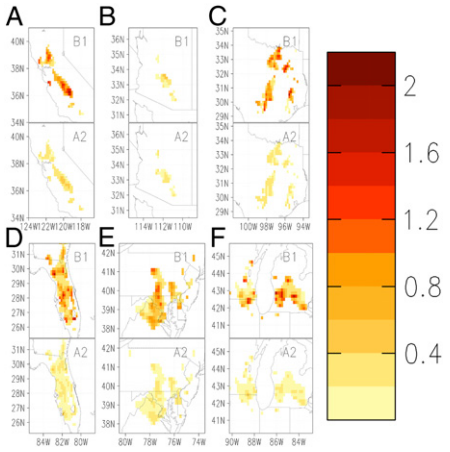

Fig. 3. Simulated JJA urban relative to greenhouse gas-induced impacts on 2-m air temperature (units are °C $°C^{-1}$). Calculations performed for the B1 urban expansion scenario relative to the RCP2.6 pathway are denoted as B1, and calculations performed for the A2 urban expansion scenario relative to the RCP8.5 pathway are denoted as A2. The following regions are shown: (*A*) California, (*B*) Arizona, (*C*) Texas, (*D*) Florida, (*E*) Mid-Atlantic, and (*F*) Chicago/Detroit urban areas. Impacts are shown only for statistically significant grid cells as described and illustrated in Fig. 1.

demand and modulation of regional-scale precipitation) when implementing urban adaptation strategies, a topic that has received scarce attention to date (27). These results emphasize regions (e.g., Florida) where tradeoff analysis among various approaches is necessary to evaluate adaptation strategies and extend discussion beyond the warm season to comprehensively characterize seasonally specific effects. Because impacts on energy demand will differ by season, geography, adaptation choice, and degree of deployment (i.e., it is unlikely that 100% deployment of the adaptation strategies examined here will occur), it is important to illustrate interseasonal changes in energy demand for less than complete deployment. For example, although cool roofs can lower energy demand during summer, a significant portion of energy savings is lost during winter because of increased heating requirements (28) (Table 2 and *SI Appendix*, Table S3). [For every 1 °C of environmental warming, cooling energy demand increases by 5–20%. For every 1 °C of environmental cooling, demand for heating energy increases by 3–15%. Variability in demand reveals differing assumptions of enhanced building equipment technology market penetration. Infrastructure investments to 2100 for energy demand were not taken into account (28).] The winter energy penalty can be lowered by adoption of a strategy that perfectly offsets urban-induced summertime warming (rather than exceeding it), albeit at a cost of decreased summertime savings (*SI Appendix*, Table S4). Although summer energy savings would decrease, such an approach could have the added benefit of reducing negative hydroclimatic consequences. By assuming linearity between the degree of adaptation deployment and cooling effect, our analysis omits inherent system nonlinearities, highlighting the need for place-based, high-resolution, cloud-resolving simulations (29) at climatic timescales with varying levels of adaptation deployment.

Our approach explicitly accounts for the individual contributions of urban and greenhouse gas impacts separately, emphasizing the significance of each agent for all megapolitan areas investigated, but it omits interactions among them; therefore, future work is required to address potential nonlinear impacts. Globally, the loss of trees and expansion of grassland contributed to a cooling of observed and projected future mean and maximum daily temperatures (30). Incorporating global land use change scenarios that include nonurban dynamics could yield unexpected

Table 2. Average JJA near-surface temperature difference (urban expansion/adaptation scenario minus control) for urban and greenhouse gas-induced (mean of 2079–2099 minus mean of 1990–2010) climate change for each of the statistically significant urbanized areas outlined in Fig. 1

	ΔT_{URB}* (°C); ΔT_{GHG}† (°C)	ΔE_{URB}‡ (%); ΔE_{GHG}§ (%)
California		
A2	1.29; 5.51	+ (6–26); + (28–110)
B1	0.69; 0.99	+ (3–14); + (5–20)
Cool roofs	−1.45	− (7–29)
Green roofs	−0.24	− (1–5)
Green–albedo roofs	−1.66	− (8–33)
Arizona		
A2	0.94; 4.86	+ (5–19); + (24–97)
B1	0.26; 1.18	+ (1–5); + (6–24)
Cool roofs	−0.47	− (2–9)
Green roofs	−0.15	− (1–3)
Green–albedo roofs	−0.80	− (4–16)
Texas		
A2	1.15; 5.24	+ (6–23); + (26–105)
B1	0.71; 1.14	+ (4–14); + (6–23)
Cool roofs	−1.24	− (6–25)
Green roofs	−0.46	− (2–9)
Green–albedo roofs	−1.46	− (7–29)
Florida		
A2	0.81; 4.79	+ (4–16); + (24–96)
B1	0.51; 0.97	+ (3–10); + (5–19)
Cool roofs	−0.41	− (2–8)
Green roofs	−0.21	− (1–4)
Green–albedo roofs	−0.46	− (2–9)
Mid-Atlantic		
A2	1.15; 6.52	+ (6–23); + (33–130)
B1	0.77; 1.54	+ (4–15); + (8–31)
Cool roofs	−1.80	− (9–36)
Green roofs	−1.19	− (6–24)
Green–albedo roofs	−2.02	− (10–40)
Chicago/Detroit		
A2	1.13; 7.57	+ (6–23); + (38–151)
B1	0.78; 1.45	+ (4–16); + (7–29)
Cool roofs	−1.37	− (7–27)
Green roofs	−0.85	− (4–17)
Green–albedo roofs	−1.49	− (7–30)

Also shown are projected changes on energy demand (28) for those regions.

*Urban expansion/adaptation scenario minus control.

†Greenhouse gas-induced (mean of 2079–2099 minus mean of 1990–2010) climate change.

‡Projected changes on energy demand (28) for urban-induced climate change.

§Projected changes on energy demand (28) for greenhouse-gas-induced climate change.

results given that, rather than simply countervailing, competing forcing agents between land use change and greenhouse gases show complex, nonadditive properties that result in otherwise indeterminable spatial patterns of change (11, 30, 31).

Notwithstanding the spectrum of expansion scenarios and adaptation strategies explored here, additional approaches requiring investigation include incorporation of permeable surfaces, which can reduce peak storm water runoff, thereby promoting more natural stream flows and fewer incidents of combined sewer overflows because of a less flashy urban environment, and seasonally adjustable cool roofs, with reflective properties that regulate based on season, thereby negating the wintertime energy penalty discussed previously. In general, prioritizing urban adaptation measures requires tradeoff assessment (25, 32) that examines the potential for multiple benefits for people and ecosystems (e.g., improved building energy efficiency, transportation technology, and judicious use of vegetation to stabilize temperatures in water-limiting environments).

Our intent was not to rate particular strategies for urban adaptation, but it was to enrich the ongoing debate by highlighting the importance of incorporating urban expansion in a realistic way, along with feedbacks to the climate system, in integrated assessment models and earth system models and emphasize the significance of geographically appropriate, rather than universal, adaptation strategies. These insights into the effect of urban adaptation have global implications. Other than Europe, every region of the world experienced urban expansion at an average annual rate >3% from 1970 to 2000 (33). By 2030, a 185% increase in global urban area is anticipated, with roughly one-quarter of that increase expected to occur in China and India alone (34). Over the same time period, Africa is expected to see the greatest proportional increase in urban land (nearly 600%). Urban expansion within these areas will almost certainly be highly concentrated, potentially exposing highly vulnerable populations to land use-driven climate change.

Materials and Methods

WRF Modeling System. We have used the advanced research version of the WRF (version 3.2.1) (14) for all modeling simulations. WRF is a fully compressible, nonhydrostatic, open-source code (www.wrf-model.org/index.php) with broad use ranging from urban to renewable energy applications (15, 16). The four-layer Noah land surface model (widely used in the climate modeling community; for example, as part of the North American Regional Climate Change Assessment Program; http://narccap.ucar.edu/data/rcm-characteristics.html), with recent improvements in snow cover and energy budget representation (35), was used to simulate soil temperature and moisture after model initialization. Urban-related processes were treated by use of a single-layer urban canopy model, accounting for shadowing from and reflection of buildings resulting from canyon orientation and diurnal change of solar azimuth angle, reduction of open sky caused by decreased sky view factor, anthropogenic heating, and biophysical representation (e.g., albedo, heat capacity, and conductivity) of building structures (i.e., roofs and walls) and roads (15, 36).

Initial and boundary data (winds, humidity, geopotential, soil moisture, and temperature) were obtained from the Research Data Archive that is maintained by the Computational and Information Systems Laboratory at the National Center for Atmospheric Research, which is sponsored by the National Science Foundation. The original data are available from the Research Data Archive (http://rda.ucar.edu) in dataset number ds083.2 (US National Centers for Environmental Prediction; http://rda.ucar.edu/datasets/ds083.2/). We have used US National Centers for Environmental Prediction Final Analyses data, which are available on a 1° × 1° global grid starting in 1999, with a 6-h temporal frequency. A detailed inventory of setup options is presented in *SI Appendix,* Table S2.

WRF Simulations. Multiyear simulations were conducted for the full suite of expansion and adaptation scenarios (*SI Appendix,* Table S1) at 20-km grid spacing and encompassed the continental United States as well as southern Canada, the northern one-half of Mexico, and portions of the Atlantic and Pacific Oceans. The simulated domain covered a surface area of 6,200 (310 points in the west–east direction) × 4,000 km (200 points in the north–south direction). The analysis time for all experiments was from January 1, 2001 to December 31, 2008 (i.e., 8 y). To reduce sensitivity to initial conditions, each scenario was repeated three times (i.e., three ensemble members), resulting in 24 simulation y per ensemble. Individual ensemble members differ according to initial start time: member 1 (for each scenario) was initialized on January 1, 2000; member 2 (for each scenario) was initialized on July 1, 2000; and member 3 (for each scenario) was initialized on January 1, 2001. The spin-up time for member 1 is, therefore, 1 y; the spin-up time for member 2 is 6 mo, and there is no spin-up time for member 3. When illustrating ensemble mean differences among expansion/adaptation scenarios, the corresponding members for each scenario were averaged.

Statistical Significance. To examine statistical significance of simulated results, we use the pairwise comparison test (37), which uses binomial probability theory to quantify the probability of K occurrences of an event in N-independent trials:

$$\frac{N!}{K!(N-K)!}p^K q^{N-K}. \quad [1]$$

In Eq. **1**, N expresses the number of possible opportunities for an event to occur, K represents the actual number of occurrences for the event, p signifies the probability of occurrence (for our analysis, the chance of occurrence is one of two or 0.5), q denotes the probability of nonoccurrence ($1 - p = 0.5$), and finally, ! represents the factorial operation.

Here, 8 y of simulations were conducted, with three ensemble members in total, resulting in a sample of 24 y (or 24 spring periods, 24 summer periods, etc.). For any specific grid cell, the probability that all 24 pairs of realizations will produce a trend of the same signal (i.e., A2 ICLUS urban expansion resulting in warming relative to control) as the mean signal by chance is $1/(2^{24})$ (significantly less than 1%). Similarly, for any particular grid cell, the probability that 23 (or more) pairs of realizations will produce a trend of the same signal as the mean signal by chance is $24/(2^{24})$ (or about 0.00000149). For any particular grid cell, the probability that 22 (or more) pairs of realizations will produce a trend of the same signal as the mean signal by chance is about 0.0000179; for 21 (or more) pairs, the chance is about 0.000139.

Our analyses use more stringent criteria than warming of the same signal as the mean trend by requiring a warming trend greater than 0.10 °C. We define virtually certain (greater than 99% probability) differences between A2 ICLUS urban expansion and the control experiment as 19 (or more) pairs of realizations resulting in warming exceeding 0.10 °C relative to the mean signal. The probability of 19 or more such occurrences (for A2 ICLUS relative to control) producing a trend of the same signal as the mean signal by chance is 0.3%.

Statistical significance is calculated separately for each season for A2 ICLUS urban expansion relative to control. Subsequent analyses on potential adaption impacts are performed only over those areas where statistically significant differences (greater than 99% probability) occur.

Comparison of Urban with Greenhouse Gas-Induced Climate Change. To compare urban relative to estimated future greenhouse gas-induced climate change, Lawrence Livermore National Laboratory (LLNL)-Reclamation-Santa Clara University (SCU) bias-corrected statistically downscaled climate projection data derived from the World Climate Research Program's Coupled Model Intercomparison Project Phase 5 multimodel dataset were obtained. These data are stored and served at the LLNL Green Data Oasis (http://gdo-dcp.ucllnl.org/downscaled_cmip_projections/dcpInterface.html#About).

We obtained multimodel projections corresponding to low- (emissions pathway: RCP2.6) and high-emission (emissions pathway: RCP8.5) trajectories from 25 and 35 Global Climate Models, respectively, of mean temperature change for a modern day period (1980–2010) and a future period (2079–2099). These time slices correspond to the period of urban area representation used in the control and future urban landscape. For each emissions pathway, the degree of warming relative to the 1990–2010 average was calculated for each representative urban area. Direct comparison with WRF simulations was made after mapping the Coupled Model Intercomparison Project Phase 5 data to the relatively coarser WRF simulation resolution of 0.18°.

Urban Deployment. To determine the deployment value that offsets urban-induced summertime warming (rather than exceeding it), we assume a linear relationship between deployment and cooling impact. For example, in California, the median impact of A2 ICLUS expansion on JJA near-surface temperature (i.e., A2 ICLUS minus control) is 1.31 °C. The median impact of 100% deployment of cool roofs (i.e., cool roofs minus control) is −1.47 °C (i.e., additional cooling of 1.47 °C beyond just an offset of urban-induced warming). To completely offset urban-induced warming, only cooling of 1.31 °C would be required. The quantity of deployment (in percentage terms) to offset urban-induced warming depends on the urban-induced warming and the total cooling assuming 100% deployment. Using the values above for California, the deployment required for offset of urban-induced warming is (1.31 °C/2.78 °C) ~47%. This calculation has been repeated for all areas and scenarios examined (*SI Appendix,* Table S4).

ACKNOWLEDGMENTS. We thank B. L. Turner, A. Brazel, C. A. Miller, and S. Julius for valued discussions. We also thank two anonymous reviewers, whose comments have led to an improved paper. We also thank B. Trapido-Lurie for assistance with figure preparations. M.G. was supported by National Science Foundation Grant EAR-1204774.

1. Grimm NB, et al. (2008) Global change and the ecology of cities. *Science* 319(5864): 756–760.
2. US Environmental Protection Agency (2010) *Inventory of US Greenhouse Gas Emissions and Sinks 1990–2008*. Available at http://epa.gov/climatechange/Downloads/ghgemissions/508_Complete_GHG_1990_2008.pdf. Accessed August 30, 2013.
3. Foley JA, et al. (2005) Global consequences of land use. *Science* 309(5734):570–574.
4. Georgescu M, Moustaoui M, Mahalov A, Dudhia J (2013) Summer-time climate impacts of projected megapolitan expansion in Arizona. *Nat Clim Chang* 3(1):37–40.
5. Bierwagen BG, et al. (2010) National housing and impervious surface scenarios for integrated climate impact assessments. *Proc Natl Acad Sci USA* 107(49):20887–20892.
6. *US and World Population Clock*. Available at http://www.census.gov/popclock/. Accessed December 31, 2013.
7. *Countries and Areas Ranked by Population: 2050*. Available at http://www.census.gov/population/international/data/countryrank/rank.php. Accessed August 30, 2013.
8. Weaver CP, Avissar R (2001) Atmospheric disturbances caused by human modification of the landscape. *Bull Am Meteorol Soc* 82(2):269–281.
9. Pielke RA (2001) Influence of the spatial distribution of vegetation and soils on the prediction of cumulus convective rainfall. *Rev Geophys* 39(2):151–178.
10. Mahmood R, et al. (2013) Land cover changes and their biogeophysical effects on climate. *Int J Climatol*, 10.1002/joc.3736.
11. Feddema JJ, et al. (2005) The importance of land-cover change in simulating future climates. *Science* 310(5754):1674–1678.
12. Kalnay E, Cai M (2003) Impact of urbanization and land-use change on climate. *Nature* 423(6939):528–531.
13. Lang R, Knox PK (2009) The new metropolis: Rethinking megalopolis. *Reg Stud* 43(6): 789–802.
14. Skamarock WC, et al. (2008) *A Description of the Advanced Research WRF Version 3* (National Center for Atmospheric Research, Boulder, CO.).
15. Chen F, et al. (2011) The integrated WRF/urban modeling system: Development, evaluation, and applications to urban environmental problems. *Int J Climatol* 31(2): 273–288.
16. Georgescu M, Lobell DB, Field CB (2011) Direct climate effects of perennial bioenergy crops in the United States. *Proc Natl Acad Sci USA* 108(11):4307–4312.
17. US Environmental Protection Agency (2009) *Land-Use Scenarios: National-Scale Housing-Density Scenarios Consistent with Climate Change Storylines (Final Report)* (Environmental Protection Agency, Washington, DC), EPA/600/R-08/076F.
18. Nakicenovic N, Swart R, eds (2000) *Special Report on Emissions Scenarios* (Cambridge Univ Press, Cambridge, United Kingdom).
19. Fry J, et al. (2011) Completion of the 2006 national land cover database for the conterminous United States. *Photogramm Eng Remote Sensing* 77(9):858–864.
20. Georgescu M, Mahalov A, Moustaoui M (2012) Seasonal hydroclimatic impacts of Sun Corridor expansion. *Environ Res Lett* 7(3):034026–034035.
21. Imhoff ML, Zhang P, Wolfe RE, Bounoua L (2010) Remote sensing of the urban heat island effect across biomes in the continental USA. *Remote Sens Environ* 114(3): 504–513.
22. Jacobson MZ, Ten Hoeve JE (2012) Effects of urban surfaces and white roofs on global and regional climate. *J Clim* 25(3):1028–1044.
23. Dominguez F, Villegas JC, Breshears DD (2009) Spatial extent of the North American monsoon: Increased cross-regional linkages via atmospheric pathways. *Geophys Res Lett* 36(7):L07401.
24. Koster RD, et al. (2004) Regions of strong coupling between soil moisture and precipitation. *Science* 305(5687):1138–1140.
25. Viguié V, Hallegatte S (2012) Trade-offs and synergies in urban climate policies. *Nat Clim Chang* 2(5):334–337.
26. Stone B, Vargo J, Habeeb D (2012) Managing climate change in cities: Will climate actions plans work? *Landsc Urban Plan* 107(3):263–271.
27. Taha H (2013) Meteorological, emissions and air-quality modeling of heat-island mitigation: Recent findings for California USA. *Int J Low-Carbon Tech*, in press.
28. Karl TR, Melillo JM, Peterson TC, eds (2009) *Global Climate Change Impacts in the United States* (Cambridge Univ Press, Cambridge, United Kingdom).
29. Georgescu M, Moustaoui M, Mahalov A, Dudhia J (2011) An alternative explanation of the semiarid urban area "oasis effect." *J Geophys Res* 116(D24):D24113.
30. Christidis N, Stott PA, Hegerl GC, Betts RA (2013) The role of land use change in the recent warming of daily extreme temperatures. *Geophys Res Lett* 40(3):589–594.
31. Jones AD, Collins WD, Torn MS (2013) On the additivity of radiative forcing between land use change and greenhouse gases. *Geophys Res Lett* 40(15):4036–4041.
32. Nelson E, et al. (2009) Modeling multiple ecosystem services, biodiversity conservation, commodity production, and tradeoffs at landscape scales. *Front Ecol Environ* 7(1):4–11.
33. Seto KC, Fragkias M, Güneralp B, Reilly MK (2011) A meta-analysis of global urban land expansion. *PLoS One* 6(8):e23777.
34. Seto KC, Güneralp B, Hutyra LR (2012) Global forecasts of urban expansion to 2030 and direct impacts on biodiversity and carbon pools. *Proc Natl Acad Sci USA* 109(40): 16083–16088.
35. Ek MB, et al. (2003) Implementation of Noah land surface model advances in the National Centers for Environmental Prediction operational mesoscale Eta model. *J Geophys Res* 108(D22):8851.
36. Kusaka H, Kimura F (2004) Thermal effects of urban canyon structure on the nocturnal heat island: Numerical experiment using a mesoscale model coupled with an urban canopy model. *J Appl Meteorol* 43(12):1899–1910.
37. von Storch H, Zwiers FW (2002) *Statistical Analysis in Climate Research* (Cambridge Univ Press, New York).